Analysis of High-Resolution Spectra From a Hybrid Interferometric/Dispersive Spectrometer

Phyllis Ko,[1] Jill R. Scott,[2] and Igor Jovanovic[1,*]

[1] *The Pennsylvania State University, University Park, PA 16802, USA*

[2] *Idaho National Laboratory, Idaho Falls, ID 83415, USA*

compiled: April 20, 2015

To fully take advantage of a low-cost, small footprint hybrid interferometric/dispersive spectrometer, a mathematical reconstruction technique was developed to accurately capture the high-resolution and relative peak intensities from complex patterns. A Fabry-Perot etalon was coupled to a Czerny-Turner spectrometer, increasing spectral resolution by an order of magnitude without the commensurate increase in spectrometer size. Measurement of the industry standard Hg 313.1555/313.1844 nm doublet yielded a ratio of 0.682 with 1.8% error, which agreed well with an independent measurement and literature values. The doublet separation (29 pm), is similar to the U isotope shift (25 pm) at 424.437 nm that is of interest to monitoring nuclear nonproliferation activities. Additionally, the technique was applied to a LIBS measurement of the mineral cinnabar (HgS) and resulted in a ratio of 0.681. This reconstruction method could enable significantly smaller, portable high-resolution instruments with isotopic specificity, benefiting a variety of spectroscopic applications.

OCIS codes: (120.2230) Fabry-Perot; (300.6320) High-resolution spectroscopy; (110.2650) Fringe analysis; (020.3690) Line shapes and shifts; (070.4790) Spectrum analysis; (300.6365) Laser induced breakdown spectroscopy.

http://dx.doi.org/10.1364/XX.99.099999

Numerous scientific, medical, industrial, and verification applications demand high-resolution spectral measurements, which can be accomplished using Fabry-Perot (FP) interferometry, among other methods. Recently, FP interferometry has been adopted in pulsed measurements via laser-induced breakdown spectroscopy (LIBS) [1]. Spectra from laser-produced plasmas are commonly measured by use of angular dispersion, such as in Czerny-Turner (CT) or echelle spectrometers [2, 3]. In LIBS, high-resolution measurements are especially valuable for measurements of isotope ratios, where the typical isotopic shifts are of order a few to several tens of picometers. Currently, isotopic specificity of rapid, economical techniques is highly sought for nuclear safeguards and non-proliferation applications. Development of LIBS methods [4, 5] to detect and monitor facilities for illicit activities (*e.g.*, undeclared isotope enrichment) is critical to risk preparedness. However, high-resolution isotope measurements presently require very large (few-meter scale) CT spectrographs [2] and echelle spectrographs with complex instrument functions and limited dynamic range [3]. More portable, simple, and cost-effective options are desirable in field applications. A practical alternative is an inexpensive, compact FP etalon coupled to a much lower resolution CT spectrometer [1]. This hybrid approach increases the instrument resolution by an order of magnitude, and can achieve the required high resolution at up to one-tenth of the size and one-fifth of the cost of available alternatives.

A diagram of the apparatus used is shown in Fig. 1. A FP etalon is comprised of two partially transmissive mirrors that produce a circularly symmetric transmission pattern dispersed over many pixels, even for a single wavelength. These ringed fringe patterns exhibits angular and spectral dependence arising from constructive and destructive interference. A broad and complex spectrum incident on the FP etalon may produce a transmission pattern that cannot be uniquely reconstructed. This is due to degeneracy inherent in the interference pattern produced by the etalon, which exhibits a characteristic periodicity and wavelength-angle coupling, whereby an identical phase shift can be produced by different combinations of wavelength and transmission angle. This degeneracy can be broken by coupling the etalon to a dispersive spectrometer, which provides an additional angular dispersion [1]. In this approach, a lens is used to produce the far field of the FP etalon output at the entrance slit of the spectrometer. The entrance slit of the spectrometer is centered on the beam axis and acts as an aperture, sampling the circular pattern along its diameter to transmit an essentially 1-D symmetric sample of the pattern. The image transmitted into the spectrometer is angularly dispersed (*e.g.*, by a diffraction grating in a CT spectrometer) and subsequently imaged by a 2-D detector array (Fig 2(a)). Thus,

* Corresponding author: ijovanovic@psu.edu

the high-resolution spectral information is encoded on the axis parallel to the spectrometer slit (*i.e.*, orthogonal to the dispersion plane of the spectrometer). The resolution that can be achieved is governed by the quality of the etalon and the sampling performed by the 2-D pixelated detector. Rapid and robust methods are desired for accurate, high resolution reconstruction of the spectra from this type of hybrid measurement to accommodate applications such as LIBS.

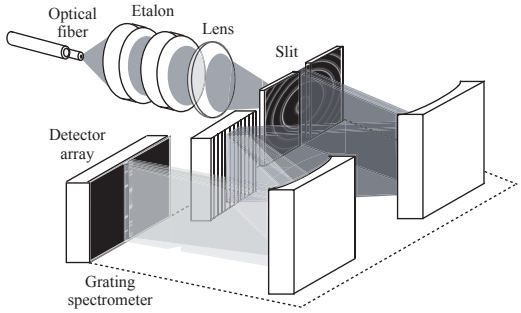

Fig. 1. Schematic diagram of experimental setup.

The production of the interference ring pattern by the FP etalon can be described as

$$B(\theta) = \int_0^\infty T(\theta,\lambda)A(\theta,\lambda)d\lambda, \tag{1}$$

where $A(\theta,\lambda)$ is the spectrally and angularly dependent intensity of the light incident on the etalon and $B(\theta)$ is the spectrally integrated intensity of the transmitted light. The FP etalon transmission function is

$$T(\theta,\lambda) = \left(1 + F\sin^2\left(2\pi d\, n/\lambda\cos\theta\right)\right)^{-1}, \tag{2}$$

where F is the coefficient of finesse, given by $F = 4R/\left(1-R\right)^2$ where R is the etalon reflectivity, d is the separation of the etalon mirrors, n is the refractive index in the space between the mirrors, λ is the wavelength, and θ is the angle measured with respect to the etalon axis. In a typical FP optical arrangement, the transmission pattern is measured in the focal plane of a lens (far field). The fringe pattern measured in this way is comprised of concentric rings of light corresponding to the angularly and spectrally dependent interference maxima arising from propagation through the FP etalon. The maxima appear when the condition $\cos\left(\theta\right)/\lambda = k\pi/\left(2\pi dn\right)$ is met (where k is an integer). Degeneracy arising from the coupling of angle and wavelength can be broken by introduction of angular dispersion, which leads to the measurement of

$$B(\theta,\lambda) = T(\theta,\lambda)A(\theta,\lambda). \tag{3}$$

Here, $B(\theta,\lambda)$ represents the recorded 2-D interference pattern. The measurement of this pattern is typically limited by the available spectral resolution, which is dictated by the properties of the arrangement used to produce dispersion and the size of the detector pixels. At any wavelength λ_0, the quantity measured is

$$B(\theta,\lambda)|_{\lambda=\lambda_0} = \int_{\lambda_0-\epsilon/2}^{\lambda_0+\epsilon/2} T(\theta,\lambda)A(\theta,\lambda)d\lambda, \tag{4}$$

where ϵ is the spectral resolution at wavelength λ_0. It is assumed for the purpose of this analysis that the resolution in the angular direction (θ) is sufficient to accurately measure the shape of $B(\theta,\lambda)|_{\lambda=\lambda_0}$. It is further assumed that light incident on the etalon does not exhibit angular dependence of the spectrum, so that the angular dependence of $A(\theta,\lambda)$ arises solely from the nonuniform angular intensity profile and $A(\theta,\lambda) = A(\theta)A(\lambda)$. The light incident on the etalon exits an optical fiber, and the Gaussian model chosen for the angular dependence of the intensity distribution is

$$A(\theta) = A_0\exp\left(-(\theta-\theta_0)^2/w^2\right) + C, \tag{5}$$

where A_0 is the peak intensity of the Gaussian envelope, θ_0 is the angle corresponding to the etalon axis, C is a constant, and w is the width of the distribution envelope [7]. The envelope function can be used to correct the measured FP pattern for its angular drop in intensity by fitting it to the Gaussian envelope $A(\theta)$.

This model of the measurement can be used for reconstructing the high-resolution features in the input spectrum directly from the measured pattern produced from the hybrid FP-dispersive instrument, without making additional assumptions regarding the shape of the spectrum, according to the method that is described as follows.

In a real measurement, the discretization and normalization (to the best-fit envelope function $A(\theta)$) of the measured transmission pattern in the neighborhood of the wavelength λ_0 yields the vector

$$\mathbf{B}_\theta = \mathbf{T}_{\theta,\lambda}\mathbf{A}_\lambda. \tag{6}$$

Here, $\mathbf{T}_{\theta,\lambda}$ is the transmission matrix constructed by discretization of Eq. (2), and $\mathbf{A}_\lambda$ is the vector representing the spectrum in the vicinity of the wavelength λ_0. The high-resolution spectrum can then be reconstructed as

$$\mathbf{A}_\lambda = \mathbf{T}_{\theta,\lambda}^{-1}\mathbf{B}_\lambda, \tag{7}$$

which is, in practice, reduced to finding the least-squares solution to this inverse problem.

The reconstruction method was applied to data collected from a hybrid FP instrument that used a 550 mm focal length imaging spectrometer (Horiba Jobin Yvon) equipped with a 1800 mm^{-1} grating and a 1024×1024 pixel array iStar ICCD (Andor) composed of 13 µm pixels. Coupled to the entrance of the spectrometer was a FP etalon (SLS Optics custom model). Light was transported to the etalon by a multimode 400 µm core diameter optical fiber (Ocean Optics). Fiber-optic connector, etalon, and lens were affixed in a cage setup, with multi-axis adjustments to enable accurate alignment of the circular transmission pattern to the spectrometer slit. A

25 mm diameter lens with a focal length of 100 mm was used to focus the output of the etalon onto the entrance slit of the spectrometer. The light source used was an Hg(Ar) calibration pen lamp (Oriel).

The FP etalon was coupled to the entrance slit of the spectrometer to produce fringes, as shown in Fig. 2(a). The section of the spectrum corresponding to the 313.1555/313.1844 nm doublet was summed along the horizontal axis to obtain the 1-D profile of the transmitted intensity, shown in Fig. 2(b). Peaks of the same order, on both sides of the optical axis, were co-added to improve the signal-to-noise ratio. A Gaussian envelope function was fit to the fringes exhibiting a characteristic double-peaked shape to obtain the $A(\theta)$ correction, as shown in Fig. 2(c). The normalized transmitted intensity pattern is shown in Fig. 2(d).

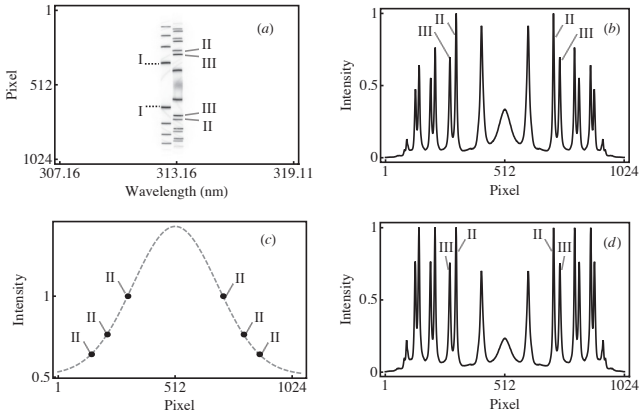

Fig. 2. (a) Measured pattern corresponding to the (I) 312.5674 nm line and (II) 313.1555/(III) 313.1844 nm doublet; (b) 1-D integrated profile of doublet; (c) intensity envelope function for (II) 313.155 nm (dots – experimental data; dashed line – fit to Eq. (5)); (d) normalized 1-D profile.

It is necessary to calibrate the angular axis before formulating the instrument function. This calibration was performed using the neighboring 312.5674 nm line (Fig. 2(a)). The angular position of highest intensity (peak) in the fringe profile was used to perform the calibration in Fig. 3. Since the paraxial approximation is valid, the calibration can be described by a linear function, also shown in Fig. 3. The region of the fringes selected for this fit did not include the area near the optical axis, or the outermost fringes, which may exhibit distortions due to their low intensity and possible optical aberrations.

Next, the instrument function for the 313 nm doublet was determined. The ranges of θ and λ used to construct the instrument function were 20 mrad $< \theta <$ 32 mrad and 313.106 nm $< \lambda <$ 313.234 nm, respectively. The etalon had air-spaced ($n = 1$) mirrors separated by a distance of $d = 0.44$ mm. The etalon reflectivity ($R = 0.73$) was determined by fitting the measured intensity profile to the known FP etalon transmission function, Eq. (2), as shown in Fig. 3.

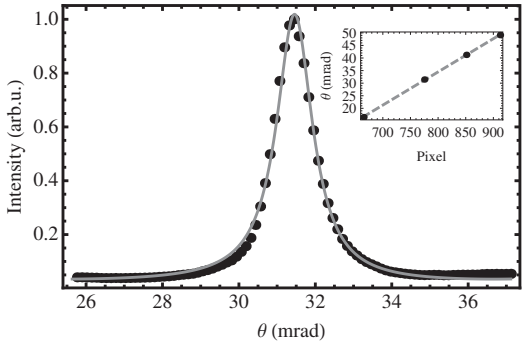

Fig. 3. Best-fit (solid line) of the measured 312.5674 nm first-order interference peak by Eq. (2) yields the reflectivity of the etalon ($R = 0.73$). Experimentally measured points are shown as black markers. Inset shows calibration of the angular (θ) axis using the location of four 312.5674 nm constructive interference peaks (black markers), The linear fit is shown as a dashed line.

Interpolation between points and increased sampling of the experimental spectrum was performed prior to reconstruction of the source spectrum, $\mathbf{A}_\lambda$. The least-squares solution to the system of linear equations associated with Eq. (7) could have been used to reconstruct $\mathbf{A}_\lambda$. However, Eq. (7) is an example of a problem where $\mathbf{T}_{\theta,\lambda}$ is an ill-conditioned matrix [6]. Hence, the pseudoinverse $\mathbf{T}^+_{\theta,\lambda}$ of the matrix was used to calculate a least-squares solution to the system of equations using

$$\mathbf{T}^+_{\theta,\lambda}\mathbf{B}_\theta = \mathbf{A}_\lambda. \tag{8}$$

The pseudoinverse solution was implemented in Mathematica (Wolfram Research) using the function `pseudoinverse`. Because of the ill-condition of the matrix $\mathbf{T}_{\theta,\lambda}$, it was necessary to specify the tolerance parameter. The singular values matrix are the non-negative square roots of the eigenvalues of $\mathbf{T}^*_{\theta,\lambda}\mathbf{T}_{\theta,\lambda}$, where $\mathbf{T}^*_{\theta,\lambda}$ is the conjugated transposed matrix. Singular values smaller than the product of the tolerance and the largest singular value of $\mathbf{T}_{\theta,\lambda}$ are omitted [9]. In practice, the choice of tolerance controls the influence of smaller singular values in the composite error of the reconstruction, and is a trade-off between reducing round-off error at the expense of a larger residual. A tolerance of 0.1 was used throughout the analysis to yield the optimal approximation to the solution.

Minimization of the residual error of the reconstruction was the next step. The widths of Hg lines from a low pressure discharge calibration lamp are approximately 1 pm [3]. The width of the reconstructed spectrum is dictated primarily by the reflectivity R. Because the widths are narrow compared to the instrument function, an accurate reconstruction assuming this experimentally determined reflectivity was not possible. By assuming a broader source spectrum, it was possible to minimize residual error in the spectral reconstruction. A reflectivity value of $R_\alpha = \alpha R$, where α is a multiplicative constant of R that minimizes the resid-

ual error, $\| \mathbf{B}_\theta - \mathbf{T}_{\lambda,\theta}\mathbf{A}_\lambda \|$ was assumed. An optimal value $\alpha = 1.16$, obtained by scanning a range of values $1.04< \alpha <1.31$, was utilized to minimize the residual error of the reconstruction.

The final reconstruction results from the hybrid instrument is shown in Fig. 4 and summarized in Table 1. Validation of the reconstructed hybrid instrument spectrum was performed by comparing the results with those acquired with a high-resolution echelle spectrometer (DEMON, Lasertechnik Berlin) using the same Hg(Ar) lamp. The DEMON results are also provided in Fig. 4 and Table 1, along with literature values [8].

Averages reported in Table 1 are based on 10, 5, and 20 spectra for sources 1, 2, and 3, respectively. The reconstructed peak wavelengths are 313.156 nm and 313.185 nm for the Hg doublet, and agree well with actual values. While the resolution is not as high for the hybrid instrument, the spectra are similar (Fig. 2) and give a very similar ratio accuracy (Table 1).

Table 1. Peak ratios of the 313 nm doublet of a Hg(Ar) calibration lamp measured by different sources. The same lamp is measured by method 1 and 2.

	Ratio	Uncert.(%)	$\lambda/\Delta\lambda$
1. Hybrid device	0.682	1.8	~37,000
2. DEMON	0.681	2.4	~75,000
3. Ref. [8]	0.687	7.2	N/A

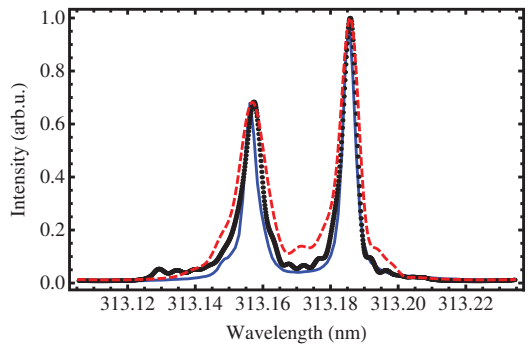

Fig. 4. (Color online) Reconstructed source spectrum of 313 nm doublet (black, dotted), compared to DEMON measurement (blue, solid) and LIBS of HgS (red, dashed).

To further explore the utility of this spectral reconstruction method, it was applied to the analysis of LIBS data from the mineral cinnabar (HgS) acquired with a different hybrid spectrometer [1]. In this case, plasma was generated by 1064 nm laser pulses at 25 mJ per pulse, and the emission light was coupled into a fiber optic connected to an FP attached to a 500 mm CT spectrometer with a 512×512, 24 µm/pixels detector array. The spectrum was collected from the accumulation of 600 laser pulses at a rate of 10 Hz and under 10 Torr He atmosphere, which is the optimum pressure for the Hg 313 nm doublet [1]. The reconstructed doublet, shown in Fig. 4, exhibits a ratio of 0.681 and is in good agreement with values reported in Table 1. Peak broadening in the LIBS spectrum is due to plasma dynamics [10].

Because only a fraction of light from each wavelength is analyzed, part of the signal is sacrificed. Mathematical summation of light from different orders of each wavelength, which is beyond the scope of this Letter, could improve signal quality. For low-light applications, a high repetition rate laser may be used to speed collection time.

This spectral reconstruction approach developed for hybrid FP/dispersive spectrometers demonstrates that simple, low-cost instruments with high resolution and accurate relative peak intensities can be realized. While such instruments would be invaluable for LIBS applications requiring accurate isotope ratio measurements, the technique would enable practical instruments for high resolution field applications.

The authors thank Andrew J. Effenberger, Jr. and Elizabeth J. Judge. Research was performed under appointment to the Nuclear Nonproliferation International Safeguards Graduate Fellowship Program sponsored by the National Nuclear Security Administration's Next Generation Safeguards Initiative. Material is based upon work supported by the U.S. Department of Homeland Security under Grant Award Number, 2012-DN-130-NF0001-02. The views and conclusions contained in this document are those of the authors and should not be interpreted as necessarily representing the official policies, either expressed or implied, of the U.S. Department of Homeland Security. Research was also sponsored by the U.S. Department of Energy under DOE Idaho Operations Office Contract DE-AC07-05ID14517.

References

[1] A. J. Effenberger Jr., and J. R. Scott, Appl. Opt. **51**, B165 (2012).
[2] C. A. Smith, M. A. Martinez, D. K. Veirs, D. A. Cremers, Spectrochim. Acta B. **57**, 929 (2002).
[3] D. A. Cremers, A. Beddingfield, R. Smithwick, R. C. Chinni, C. R Jones, B. Beardsley, and L. Karch, Appl. Spectrosc. **66**, 250 (2012).
[4] C. Hanson, S. Phongikaroon, and J. R. Scott, Spectrochim. Acta B. **97**, 79 (2014).
[5] P. Ko, K. C. Hartig, J. P. McNutt, R. B. D. Schur, T. W. Jacomb-Hood, and I. Jovanovic, Rev. Sci. Instrum., **84**, 013104 (2013).
[6] J. B. Abbiss, and B. Heeg, Rev. Sci. Instrum., **79**, 123105 (2008).
[7] M. C. Hirschberger, and G. Ehret, App. Phys. B, **103**, 207 (2011).
[8] J. Reader, C. J. Sansonetti, and J.M. Bridges, Appl. Opt. **35**, 78 (1996).
[9] G. H. Golub, and C. Reinsch, Numer. Math., **14**, 403 (1970).
[10] J. R. Scott, A. J. Effenberger Jr., and J J. Hatch, Laser-induced Breakdown Spectroscopy–Theory and Applications (Springer-Verlag, 2014), Chap. 4.